Resolving the Rise and Fall of Star Formation in Galaxies
Proceedings IAU Symposium No. 373, 2023
T. Wong & W.-T. Kim, eds.
doi:10.1017/S1743921322004574

Evolution of Gas Flows over the Starburst to Post-Starburst to Quiescent Galaxy Sequence

Yang Sun[1], Gwang-Ho Lee[1,2], Ann I. Zabludoff[1], K. Decker French[3], Jakob M. Helton[1], Nicole A. Kerrison[1], Christy A. Tremonti[4] and Yujin Yang[2]

[1]Steward Observatory, University of Arizona, 933 North Cherry Avenue, Tucson, AZ 85721, USA

[2]Korea Astronomy and Space Science Institute, 776 Daedeokdae-to, Yuseong-gu, Daejeon, 305-348, Republic of Korea

[3]Department of Astronomy, University of Illinois, 1002 West Green Street, Urbana, IL 61801, USA

[4]Department of Astronomy, University of Wisconsin–Madison, 475 North Charter Street, Madison, WI 53703, USA

Abstract. Even though galactic winds are common in galaxies with starbursts or active galactic nuclei (AGN), the role of such gas flows in galaxy evolution remains uncertain. Here we examine how winds vary along a likely evolutionary sequence connecting starburst to post-starburst to quiescent galaxies. To detect the interstellar medium and measure its bulk flows, we examine the residual Na D absorption line doublet after the stellar contribution has been removed from each galaxy's spectrum. We discover that outflows diminish along this sequence, i.e., as star formation ends. We then focus on the wind behavior within the post-starburst sample, for which we have measured the time elapsed since the starburst ended (post-burst age) via detailed modeling of their star formation histories (French *et al.* 2018). Even within our post-starburst sample, the fraction of galaxies with significant winds and the average wind velocities decrease with post-burst age after controlling for stellar mass.

Keywords. ISM: jets and outflows – ISM: kinematics and dynamics – galaxies: evolution – galaxies: ISM

1. Introduction

In the local Universe, observational surveys suggest there are two main types of galaxies: star-forming and quiescent. The current understanding of this bimodality indicates that star-forming galaxies will eventually stop forming stars and evolve to the quiescent phase. Transitioning galaxies evolving between star-forming and quiescent are found in the "green valley". One rare class of transitioning galaxies is the post-starburst galaxy. This type of galaxy is believed to have experienced a burst of star formation that was halted in the past $\sim$1 Gyr (Dressler & Gunn 1983; Couch & Sharples 1987). Their optical spectra show strong Balmer absorption lines suggesting a recent starburst has occurred but are without strong nebular emission lines indicating a low current star formation rate. Even though the star formation must decline along the evolutionary sequence from starburst to post-starburst to quiescent, the reasons why star formation has stopped are still unknown.

One likely mechanism for this quenching is feedback. For current cosmological simulations of galaxy formation and evolution, feedback is required to reproduce observed galaxy baryonic mass functions and star formation efficiency (Kereš *et al.* 2009; Hopkins *et al.* 2014; Somerville & Davé 2015; Naab & Ostriker 2017, and references therein). Massive stars, supernovae, and active galactic nuclei (AGN) may be sources of negative feedback through thermal or kinetic energy transferred to the interstellar medium (ISM) in galaxies. If negative feedback processes remove the cold gas in winds (see Veilleux *et al.* 2005; King & Pounds 2015; Veilleux *et al.* 2020), star formation could rapidly end due to the removal of the fuel for star formation.

The connections between galactic outflows and star formation have been well studied in the past decades. For instance, Chen *et al.* (2010) systematically analyzed the stacked Na D line of star-forming galaxies in the SDSS DR7 survey, finding strong ISM Na D absorption lines are only prevalent in disk galaxies with high star formation rates (SFR), high SFR per unit area (ΣSFR), or high stellar mass ($M_\star$). However, none have tested how winds evolve along the galaxy evolutionary sequence where star formation is declining. Based on previous findings that higher outflow detection rates and larger Na D EWs prefer to locate at higher SFR and $M_\star$ spaces, we expect that there should be decline in winds over this sequence. Therefore, this work aims to build a star formation declining sequence from starburst to post-starburst to quiescent galaxy in the local Universe ($0.010 < z < 0.325$) and tests for wind evolution along it. Moreover, French *et al.* (2018) (hereafter F18) modeled the star formation histories (SFHs) of their ∼500 post-starburst galaxies with post-burst ages, burst mass fraction and burst durations. These ages allow us to reveal wind evolution with a more highly time-resolved view.

We use the spectroscopic sample of the SDSS DR12 survey (Alam *et al.* 2015) and analyze the Na I $\lambda\lambda$5890, 5896 line to trace the bulk motion of the neutral gas of starburst, post-starburst and quiescent samples. In this text we report the current results on how wind properties change along the first sequence and with post-burst age.

2. Building the SFR-declining galaxy evolutionary sequence

Here we briefly introduce how we built the star formation declining galaxy evolutionary sequence from the SDSS galaxy.

F18 provided a sample of 522 post-starburst galaxies with $0.010 < z < 0.325$ that are drawn from the spectroscopic sample in the Sloan Digital Sky Survey Data Release 8 (DR8, Aihara *et al.* 2011). In the equivalent widths (EWs) of the Hα and the Lick Hδ absorption line index (Hδ_A) diagram F18 selected the post-starburst sample following the selection criteria: H$\alpha < 3$ Å in the rest-frame, representing a lack of current star formation, and strong Balmer absorption line index H$\delta_A - \sigma$(Hδ_A) > 4 Å, where σ(Hδ_A) is the measurement error, representing recent starburst in the past $\sim 1 - 1.5$ Gyr.

Then we construct two different comparison samples of starburst galaxies and quiescent galaxies that represent the likely progenitors and descendants of post-starburst galaxies, respectively. We start with a parent sample of 593,807 galaxies drawn from the SDSS DR12 survey (Alam *et al.* 2015), which is at the same redshift range as post-starburst galaxies, has continua S/N≥ 10, and has galaxy properties and spectral line flux measurements from the MPA-JHU Catalogs (Kauffmann *et al.* 2003; Brinchmann *et al.* 2004; Tremonti *et al.* 2004). For the starburst galaxy sample, we require they are star-forming galaxies in the BPT diagram (Kewley *et al.* 2006), their SFRs are 5σ higher than the main-sequence and their stellar masses are within the proper range considering each post-starburst galaxy's current stellar mass and burst mass fraction. Quiescent galaxies are selected to have H$\delta_A + \delta$(Hδ_A) < 1 Å and Hα EW< 3 Å, with the intention of selecting galaxies with no current and recent star formation. We finalize the starburst sample with

https://doi.org/10.1017/S1743921322004574 Published online by Cambridge University Press

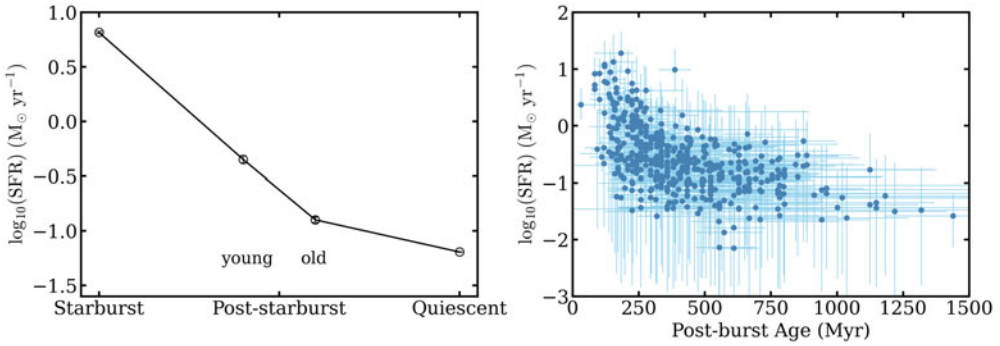

Figure 1. SFR evolves along the evolutionary sequence (left) and with post-burst age (right), which confirms that SFR declines along the evolutionary sequence we build. In the left panel, the post-starburst sample is divided into two subsamples: young (post-burst age < 400 Myr) and old (≥ 400 Myr). SFR measurements are obtained from MPA-JHU catalogs.

3306 galaxies and the quiescent sample with 72,251 galaxies. Figure 1 shows SFR of our samples declines along the whole sequence and with post-burst age.

3. Detecting neutral ISM bulk flows

In this section, we introduce how we detect neutral bulk flows and measure their properties in our three galaxy sample.

Firstly, the stellar continua are well fitted by the penalized pixel fitting (pPXF, Cappellari & Emsellem 2004; Cappellari 2017) Python code with MILES (Vazdekis *et al.* 2010) simple stellar population (SSP) models.

After obtaining the best-fit stellar continuum model, we measured the equivalent widths of both the total and the residual (after subtracting the best-fit stellar continuum model) of Na D absorption line ($\mathrm{EW_{NaD,tot}}$ and $\mathrm{EW_{NaD,exc}}$) using Monte Carlo simulation to derive the mean values and errors of $\mathrm{EW_{NaD,tot}}$ and $\mathrm{EW_{NaD,exc}}$.

The velocity of bulk flow motions (Δv) from the galaxy redshift is another important properties we measure. To do this, we apply a double Gaussian profile to fit the Na D residuals at the wavelength of 5850-5940 Å. we assume the widths of Na D are the same and the doublet flux ratio is in the range from 1 to 2, corresponding to the scenario of optically thin and thick, respectively. The shifted wavelength of the Na D excess is constrained as μ: [−20, 20]+5890 Å that corresponds to $\Delta v \sim \pm 1000$ km s^{-1}. Depending on the geometry, it is possible to see Na D emission in the case that absorbed photons are re-emitted along the line of sight. This scattering process can produce P-Cygni profiles of Na D. We do find a small fraction ($\sim 1\%$) of galaxies in our three samples showing a clear P-Cygni profile in their residual spectra. In this case, the overall profile should be fit by two double Gaussian components but Δv is measured from the blueshifted absorption component only. Then we use Monte Carlo simulation to obtain the Δv and its uncertainty, similar to what we do for EW measurement. A example of the Na D excess fitting for a post-starburst galaxy with the P-Cygni profile is shown in Figure 2.

Excluding samples without Na D ISM absorption or good velocity measurements, finally we obtain Δv measurements for 589 starburst, 202 post-starburst, and 9,711 quiescent galaxies. However, to avoid unreliable further analysis for very weak bulk flows, we further define flow-detected samples as samples with significant Na D excess ($\mathrm{EW_{NaD,exc}} - 3\sigma(\mathrm{EW_{NaD,exc}}) > 0$) or P-Cygni profile. The flow-detected sample includes 370 starburst galaxies, 164 post-starburst galaxies, and 4,598 quiescent galaxies. Hereafter we only focus on those samples with strong bulk flows.

https://doi.org/10.1017/S1743921322004574 Published online by Cambridge University Press

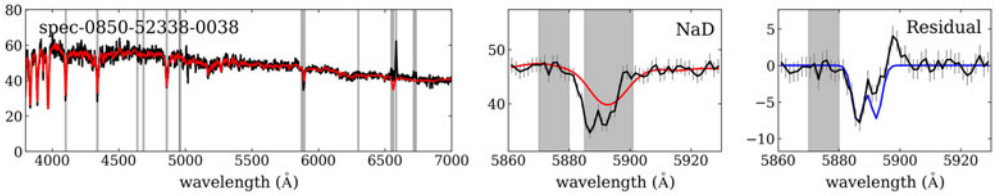

Figure 2. Example of galaxy spectral fitting. Left: the SDSS spectra of a post-starburst galaxy in the rest-frame (black) and their best-fit stellar continuum model obtained using pPXF (red). Middle: The zoom-in Na D spectra (black) with the best-fit stellar continuum models (red). Right: The Na D residual spectra (black), representing the ISM, and their best-fit double Gaussian profile (blue).The errorbars in three panels are the original flux uncertainties from the SDSS spectra. The masked regions are shown as gray areas. This post-starburst galaxy have the P-Cygni profile in the Na D residual which is composed of a blueshifted absorption component and a redshift emission component.

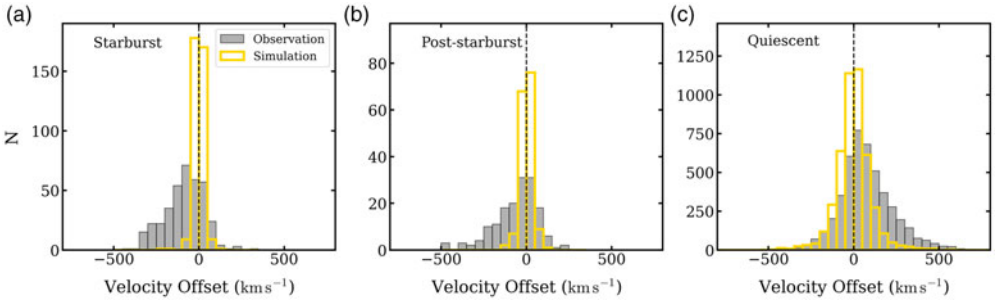

Figure 3. The histograms of Δv for the (a) starburst, (b) post-starburst and (c) quiescent sample. The observed wind distributions are displayed by gray filled histograms. The yellow open histograms represent simulated data expected from zero velocity wind and 1σ measurement error. The mean velocities and their errors of three galaxy samples from left to right are -84.6 ± 5.9 km s^{-1}, -71.8 ± 11.4 km s^{-1}, and 76.6 ± 2.3 km s^{-1}. For starburst and post-starburst samples, the distributions of observation shows significant negative velocity tails comparing with those of simulations. On the contrary, the quiescent sample has a significant positive tail.

4. Outflows in starburst and post-starburst galaxies

Assuming a possible evolutionary sequence from starburst to post-starburst to quiescent, Figure 3 shows the histograms of wind velocities for the three samples with this sequence (grey histograms). The histograms for the starburst and post-starburst samples are significantly skewed with a tail at high negative wind velocities. The mean values of wind velocities are -84.6 ± 5.9 km s^{-1} and -71.8 ± 11.4 km s^{-1} for the starburst and post-starburst samples, respectively. On the other hand, the quiescent galaxy's histogram is skewed to the positive velocities with the mean velocity of 76.6 ± 2.3 km s^{-1}. But the overall shape of the histogram is symmetric compared to the histograms for the two other samples.

To test whether these differences are statistically significant, we compare the distribution of observed wind velocities with that expected from measurement errors alone in each panel. We use the 1σ velocity measurements errors of samples and randomly made them half negative and half positive, then added to zero velocities, and compared the zero wind models (yellow histograms in Figure 3) with the observed wind distributions. For the starburst and post-starburst samples, the distributions of Δv show negative wind velocity tails exceeding the distributions expected from measurement errors alone. On the other hand, the histogram of the observed wind velocities for the quiescent galaxy sample

https://doi.org/10.1017/S1743921322004574 Published online by Cambridge University Press

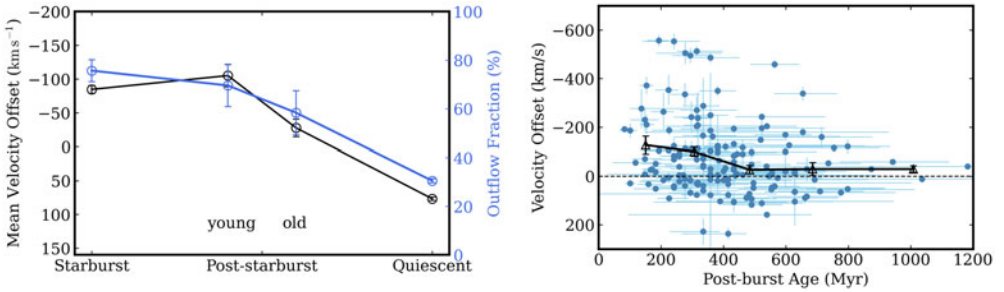

Figure 4. Left: The trends of outflow velocity (black) and outflow fraction (blue) with the evolutionary sequences, from starburst to post-starburst to quiescent galaxies. The post-starburst sample is divided into two subsamples: young (post-burst age < 400 Myr) and old (≥ 400 Myr). Outflow velocity and outflow fraction both decrease along the sequence. Right: The overall trend of wind velocity with post-burst age for the post-starburst sample without removing stellar mass dependency. The black triangles show the mean velocity in each post-burst age bin. Within the post-starburst phase, outflow velocities still decrease with post-burst age. More accurate partial-correlation analysis confirms the correlation between wind velocity and post-burst age controlling stellar mass is with 2.26σ significance. The figure is reproduced from Sun *et al.* (in prep).

shows a significant excess of positive wind velocities. Those differences are confirmed by Kolmogorov-Smirnov test (fails a KS test).

Assuming Na D excess represents the average properties from the foreground ISM in the light of sight, negative and positive wind velocities represent bulk flows of the ISM in opposite direction: negative velocities indicate outflows, while positive velocities indicate inflows. Therefore, the exceeding negative velocity tails of the starburst and post-starburst samples show that these two groups have significant strong outflows, while the positive tails of the quiescent sample suggests the presence of strong inflows.

5. Trends along the evolutionary sequence

In this section, we introduce how wind properties we derived (i.e., outflow fraction and velocities) evolve along the assumed evolutionary sequence (starburst - post-starburst - quiescent), which is the main result of Sun *et al.* (in prep). For the post-starburst sample, we further divided it into two groups: the young post-starburst group (post-burst age < 400 Myr) and the old post-starburst group (post-burst age ≥ 400 Myr).

The outflow fraction is defined as the number of galaxies with outflows as a percentage of the number of galaxies with flow. The outflow fractions for the starburst, post-starburst and quiescent sample are $76 \pm 5\%$, $65 \pm 6\%$, and $31 \pm 1\%$, respectively. The left panel of Figure 4 shows the overall trends of outflow fractions with the sequence. Dividing the post-starburst into two age groups, the outflow fraction of the young group is $70 \pm 9\%$ and that of the old one is $58 \pm 9\%$. As we mentioned in Section 4, The wind velocity decreases from the starburst sample (-84.6 ± 5.9 km s^{-1}) to the post-starburst sample (-71.8 ± 11.4 km s^{-1}), and then changes to a positive value in the quiescent stage (76.6 ± 2.3 km s^{-1}). The left panel of Figure 4 shows the velocity trend with the sequence, but here the post-starburst sample are divided into the young and old group as well. The mean wind velocity of the young post-starburst galaxy sample (-105.1 ± 16.6 km s^{-1}) is slightly higher than the value of the starburst galaxy sample, but are consistent within 1σ error. The value of the old post-starburst galaxy sample (-27.6 ± 13.0 km s^{-1}) is lower than that of the young group. Even though we do not only focus on outflows, since overall wind velocities change from more negative values to less negative values

https://doi.org/10.1017/S1743921322004574 Published online by Cambridge University Press

to positive values, we represent this trend as: outflows diminish along the evolutionary sequence.

We also test the outflow velocity evolution at the post-starburst stage. The right panel of Figure 4 visualizes the average trend of wind velocity and post-burst age. After controlling the stellar mass effect, the final Spearman partial-correlation coefficient for the trend is 0.177, with 2.26σ significance. The correlation implies that, outflows diminish with the evolution of post-starburst phase as well.

6. Conclusions

In this work, we use the Na D absorption line to analyze bulk gas motions in the ISM of ∼80,000 galaxies from the SDSS DR12 survey who follow a SFR declining galaxy evolutionary sequence, from starburst to post-starburst, to quiescent galaxies. The bulk flow are detected in all three galaxy samples, but are mainly located at high mass end ($\log(M_*/M_\odot) \geq 10$). We find a small fraction ($\sim 1\%$) of starburst, post-starburst, and quiescent with bulk flows show the P-Cygni profile. The starburst and post-starburst sample show statistically significant negative velocity tails, which means many of them have outflows. Even though the quiescent sample has positive velocity tail which represents significant inflows, inflows are weak due to the small EW of Na D excess. Outflow fractions and outflow velocities similarly decrease from starburst ($76 \pm 5\%$, $-84.6 \pm 5.9\,\mathrm{km\ s^{-1}}$) to young ($70 \pm 9\%$, $-105.1 \pm 16.6\,\mathrm{km\ s^{-1}}$) and old post-starburst ($58 \pm 9\%$, $-27.6 \pm 13.0\,\mathrm{km\ s^{-1}}$) to quiescent ($31 \pm 1\%$, $76.6 \pm 2.3\,\mathrm{km\ s^{-1}}$). Even within the post-starburst phase, outflows diminish with post-burst age. It indicates that neutral gas outflows we detected diminish with star formation over time.

References

Aihara, H., Allende Prieto, C., An, D., *et al.* 2011, *ApJS*, 193, 29
Alam, S., Albareti, F. D., Allende Prieto, C., *et al.* 2015, *ApJS*, 219, 12
Brinchmann, J., Charlot, S., White, S. D. M., *et al.* 2004, *MNRAS*, 351, 1151
Cappellari, M. 2017, *MNRAS*, 466, 798
Cappellari, M. & Emsellem, E. 2004, *PSAP*, 116, 138
Chen, Y.-M., Tremonti, C. A., Heckman, T. M., *et al.* 2010, *AJ*, 140, 445
Couch, W. J. & Sharples, R. M. 1987, *MNRAS*, 229, 423
Dressler, A. & Gunn, J. E. 1983, *ApJ*, 270, 7
French, K. D., Yang, Y., Zabludoff, A. I., *et al.* 2018, *ApJ*, 862, 2
Hopkins, P. F., Kereš, D., Oñorbe, J., *et al.* 2014, *MNRAS*, 445, 581
Kauffmann, G., Heckman, T. M., White, S. D. M., *et al.* 2003, *MNRAS*, 341, 33
Kereš, D., Katz, N., Davé, R., *et al.* 2009, *MNRAS*, 396, 2332
Kewley, L. J., Groves, B., Kauffmann, G., *et al.* 2006, *MNRAS*, 372, 961
King, A. & Pounds, K. 2015, *ARA&A*, 53, 115
Naab, T. & Ostriker, J. P. 2017, *ARA&A*, 55, 59
Somerville, R. S. & Davé, R. 2015, *ARA&A*, 53, 51
Sun, Y., Lee, G., Zabludoff, A. I., *et al.* in prep
Tremonti, C. A., Heckman, T. M., Kauffmann, G., *et al.* 2004, *ApJ*, 613, 898
Vazdekis, A., Sánchez-Blázquez, P., Falcón-Barroso, J., *et al.* 2010, *MNRAS*, 404, 1639
Veilleux, S., Cecil, G., & Bland-Hawthorn, J. 2005, *ARA&A*, 43, 769
Veilleux, S., Maiolino, R., Bolatto, A. D., *et al.* 2020, *A&AR*, 28, 2

https://doi.org/10.1017/S1743921322004574 Published online by Cambridge University Press